Australian Meteorological and Oceanographic Journal 62 (2012) 71–82

The surface heat fluxes along the eastern Pacific coast from 10°N to 40°S

José Garcés-Vargas[1,2] and Rodrigo Abarca-del-Río[1]
[1]Universidad de Concepción, Facultad de Ciencias Físicas y Matemáticas, Departamento de Geofísica, Concepción, Chile
[2]Universidad Austral de Chile, Facultad de Ciencias, Instituto de Ciencias Marinas y Limnológicas, Casilla 567, Valdivia, Chile

(Manuscript received January 2011; revised May 2012)

An adequate understanding of the ocean–atmosphere interface is important for understanding climate variability on different time scales. Thus, this research focuses on surface heat fluxes over seasonal scales and their changes during El Niño and La Niña along the eastern Pacific coast (10ºN–40ºS), consistent with oceanographic and meteorological fields. We used a wide range of up-to-date databases, new mean monthly heat air–sea fluxes (NOCS Flux Dataset v2.0) and complementary global databases (SODA reanalysis, SeaWiFS). The results reported here show that of all the fluxes contributing to net heat flux (Q_{net}), net shortwave radiation (Q_{sw}) is the term that warms and is most dominant, and latent heat flux (Q_{lat}) is the term that most contributes to cooling. Considering seasonal variability, Q_{sw} reduction due to cloud cover in the latter half of the year was associated with the presence of the Intertropical Convergence Zone and the stratus cloud deck at 10ºN–Eq and Eq–30ºS, respectively. The smaller seasonal amplitude south of 30ºS was associated with the southern coastal jet that develops along the eastern flank of the low-level circulation over the southeast anticyclonic Pacific. During El Niño and La Niña, the most significant change was observed for Q_{lat} in the first half of the year, between the equator and the Peruvian coast. Q_{lat} tended to cool (warm) during El Niño (La Niña), acting as a negative feedback. Specifically for Q_{lat}, we found that the air–sea specific humidity difference (rather than the wind) played a prominent role in both El Niño – Southern Oscillation phases. The sum of Q_{net} and the shortwave radiation that penetrates through the base of the mixed layer was compared with the sea surface temperature tendency and was discussed.

Introduction

The oceans play a fundamental role in climate by storing and transporting energy and exchanging momentum and heat across the ocean–atmosphere interface. The need for accurate climatological descriptions of the heat and momentum transfer is well recognized (e.g. Taylor 2000). In addition to the fundamental insights they provide into the physics of the ocean–atmosphere system, accurate fields of the heat fluxes are vital for modeling studies both as boundary conditions for ocean models and for verification of flux fields obtained from coupled ocean–atmosphere models. Therefore, an adequate understanding of the surface heat fluxes at the ocean–atmosphere interface is important for understanding climate variability over different timescales.

The Eastern Pacific Coast (EPC, 10ºN–40ºS, 200 km off the west coast of Central–South America, Fig. 1) hosts different ocean–atmosphere processes (Mackas et al. 2006). The EPC's northern area includes the coasts of Panama, Colombia and the north of Ecuador. At the Isthmus of Panama, an intense and narrow Panama wind jet enters the far eastern equatorial Pacific and blows offshore into the Gulf of Panama during the austral summer (Amador et al. 2006) (Fig. 2(c)) producing a cyclonic gyre and cooling surface waters at the center of the Panama Bight (Devis-Morales et al. 2008; Kessler 2006). A seasonally changing wind field, caused by the meridional migration of the intertropical convergence zone (ITCZ) (Fig. 2), controls the circulation of the basin (Rodríguez-Rubio et al. 2003). The southern region of this margin (southeastern Pacific) is composed principally of the Humboldt Current system and the most eastern part of the South Pacific

Corresponding author address: José Garcés-Vargas, Instituto de Ciencias Marinas y Limnológicas, Facultad de Ciencias, Universidad Austral de Chile, Campus Isla Teja, Valdivia, Chile
email: jgarces@docentes.uach.cl

Fig. 1. (a) Mean SST (ºC) and mean range SST (ºC), and (b) mean net surface heat flux (colour, W m^{-2}) and mean net surface heat flux uncertainty (contour, W m^{-2}) in the eastern Pacific based on NOCS v2.0. The white line shows the zone along the eastern Pacific coast (200 km off the coast). The right colour bar displayed in (a) and (b) gives the SST and net surface heat flux, respectively.

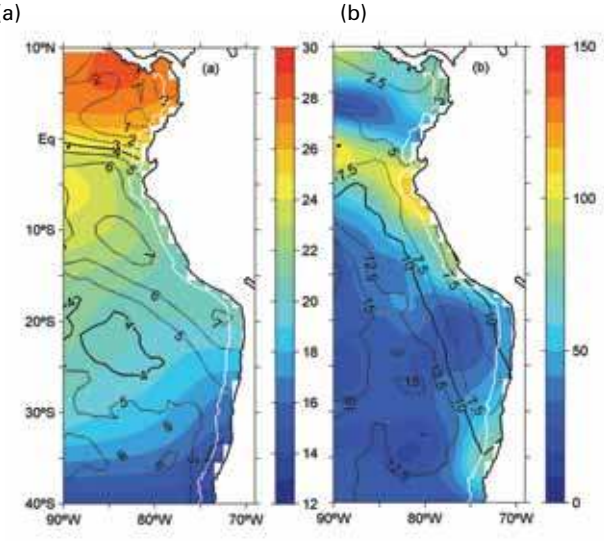

subtropical gyre (Thiel et al. 2007), which includes the coastal upwelling ecosystems of southern Ecuador, Peru and Chile. It is well known that the southeastern Pacific is characterized by a low stratus cloud deck that develops over a cold tongue (Amador et al. 2006; McPhaden et al. 2008) (Fig. 2(b)). Further south, a coastal jet off central Chile (26º–36ºS) tends to dissipate the coastal deck of stratocumulus clouds (Garreaud and Muñoz 2005; Muñoz and Garreaud 2005) (Fig. 2).

The annual mean of sea surface temperature (SST) and its range (SST maximum – SST minimum) from 1980 to 2005 along the EPC present large variability: SSTs above 26ºC (SST range < 3) and below 24ºC (SST range > 4) are found in the EPC's northern Pacific and southeastern areas, respectively (Fig. 1(a)), separated by the equatorial front. Additionally along this front, an equatorial upwelling system occurs due to Ekman transport north (or south) of the equator, which is to the right (or left) of the westward component of the southeast trade winds (Pennington et al. 2006).

The SST, as one of the main manifestations of ocean–atmosphere processes, varies due to changes in the different air–sea processes and the ocean's energy exchange (heat and momentum) across the air–sea interface (Large 2006; Peixoto and Oort 1992; Wallcraft et al. 2008). In the absence of clouds (or presence of constant cloud cover), the received surface radiation behaves semi-annually at the equator according to the twice-per-year sun translation through the equator. However, far from the equator, it behaves annually according to the once-per-year sun translation through the equator (Dobson and Smith 1985, algorithm). Thus, one might expect similar behavior for SST. However, diverse studies have shown that SST variability in the eastern equatorial Pacific is primarily annual and interannual, with both air–sea heat fluxes and advective terms being significant contributors (e.g. Borovikov et al. 2001; Kessler et al. 1998). It has also been noticed that these terms are essential in the determination of SST anomalies at the interannual timescale (Vialard et al. 2001; Wang and Fiedler 2006; Wang and McPhaden 2000).

Southeastern Pacific air–sea heat flux terms have not been studied much. Only a few publications have examined the processes responsible for the mean seasonal SST cycle, along with changes associated with El Niño – Southern

Fig. 2. Seasonal climatology of the meteorological variables in the eastern Pacific based on NOCS v2.0 (except windstress, which is obtained from SODA). (a) Total cloud amount (TCA [%]), Summer (JFM), (b) TCA, Winter (JAS), (c) sea level pressure (SLP [mb], colour) and windstress (WStress [Pa], vectors), Summer, (d) SLP (colour) and WStress (vectors), Winter. The right colour bar in each panel displayed applies. A reference arrow of the WStress is at 8ºS over the continent.

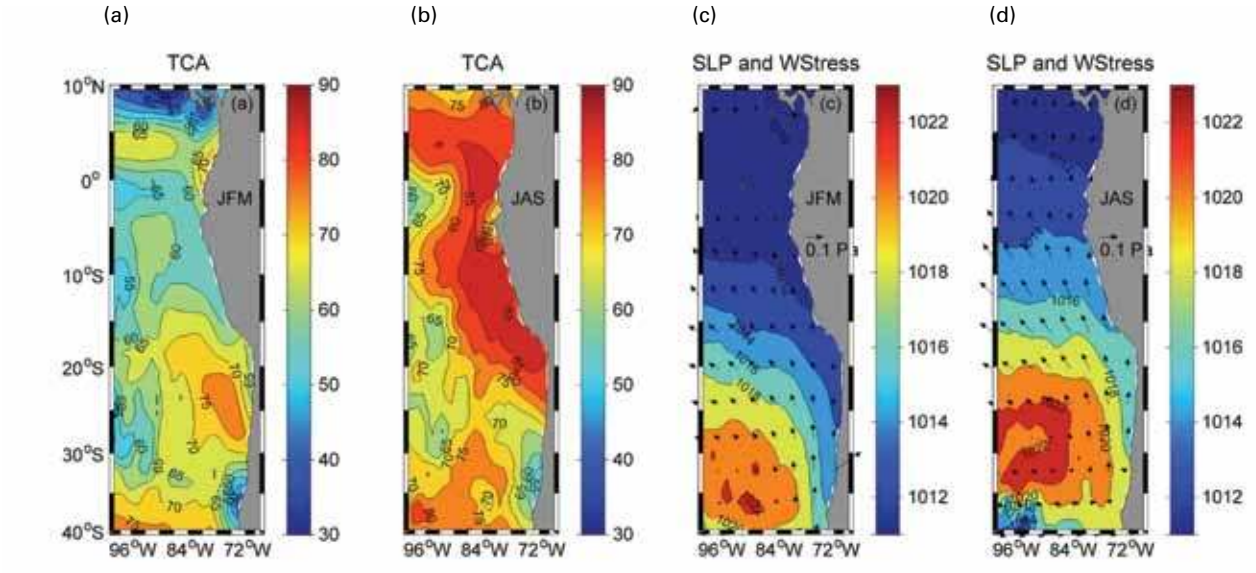

Oscillation (ENSO) events (El Niño and La Niña), and these studies have been mostly limited to small regions. Thus, for example, simulations with a straightforward local wind-driven upwelling/entrainment model have been performed to explain SST at 18°20′S–24°S off northern Chile (Iquique) (Bravo 2003), and off central Chile (Valparaiso) (Hormazabal et al. 2001). Also, using data (2000–2004) from a buoy located off northern Chile (at 20ºS, 85ºW), Colbo and Weller (2007) examined the variability of SST and the temporal evolution of the vertical structure of the upper ocean. The same buoy allowed a complete climatological study of the meteorology, surface fluxes, cloud fraction, and radiative forcing (Ghate et al. 2009). Finally, at the regional scale, a study by Takahashi (2005), including part of the EPC (Peru Current region), outlined the importance of the mixed layer depth.

Understanding seasonal and interannual surface heat flux changes is crucial to understanding climate variability over other timescales: for example, the impact of global warming on a regional scale. By complementing the scarce knowledge of this zone, we will improve prediction for the EPC region and impact other fields of knowledge. Therein lies the importance of carefully examining the air–sea processes that explain its variability.

We concentrate on the EPC because the NOCS v2.0 fluxes dataset used in this analysis contains large uncertainties mostly offshore. For example, offshore south of 5ºS, annual averages of the net heat flux uncertainties exceed 13 W m^{-2} (Fig. 1). To the north, we restrict ourselves to about the limit of influence of the ITCZ, which is a region of deep convection and intense rainfall. In addition, most of the works offshore from the eastern Pacific have been done mostly using Tropical Atmosphere–Ocean/Eastern Pacific Investigation of Climate (TAO/EPIC) moorings, i.e. in the tropics to the west of 95ºW (e.g. Cronin et al. 2006a, 2006b; Fairall et al. 2008; McPhaden et al. 2008), framed by Pan American Climate Studies, and in the subtropics, specifically 85ºW–20ºS (Colbo and Weller 2007; Ghate et al. 2009). In addition, knowledge of the EPC's variability will improve understanding of SST, which has warm biases for areas close to the South American coast according to most general circulation models, suggesting that all simulations have too few or radiatively ineffective clouds (de Szoeke et al. 2010).

This research focuses principally on the surface heat flux changes at seasonal timescales along the eastern Pacific coast, studying each of the surface fluxes that participate in the net heat flux (Q_{net}) in detail. The mixed layer is the most active zone within the water column; therefore it characterizes most of the air–sea fluxes (Cronin and Sprintall 2001). Thus, this study also examines the influence of mixed layer characteristics on air–sea exchange flux variability (e.g. shortwave radiation that penetrates through the base of the mixed layer (Q_{pen})). Given the importance of ENSO events for the ocean–atmosphere variables within the region (Caviedes 2000), we also explore their influence on surface heat fluxes. Finally, we compare the sum of Q_{net} and Q_{pen} with the SST tendency and discuss the possible processes that may explain its variability. All this is done by taking into account up-to-date meteorological and oceanographic variables.

Datasets

Subsets for the eastern Pacific coast (10ºN–40ºS, ~200 km off the west coast of Central–South America) were determined from different data products: (1) NOCS Flux Dataset v2.0; (2) Simple Ocean Data Assimilation; and (3) SeaWiFS. We used monthly means from 1980 to 2005 from (1) and (2).

NOCS Flux Dataset v2.0

We used a new monthly mean air–sea interaction gridded dataset. This new dataset, the NOCS Flux Dataset v2.0 (hereafter NOCS v2.0), is a major update of the NOCS Flux Dataset v1.1, often referred to as the 'Original SOC Flux Climatology' (Josey et al. 1998, 1999). NOCS v2.0 is based on Voluntary Observing Ships observations from the International Comprehensive Ocean–Atmosphere Data Set (ICOADS) (Worley et al. 2005). The dataset includes monthly fields of meteorological variables and fluxes, and their associated random and uncertainty estimates on a 1° spatial grid (Berry and Kent 2009).

Uncertainty estimates can be used as an indicator of the quality of the gridded values and flux estimates. The uncertainty in the annual mean heat flux was calculated by assuming that the uncertainties in the different months are uncorrelated, and the mean of the monthly uncertainties was reduced by $\sqrt{n}$ accordingly (where n is the number of months with ground truth data) (Berry and Kent 2011). Here, we computed the monthly net heat flux uncertainty by adding the total uncertainties for the different terms in quadrature, which is the square root of the errors of each of the terms involved in the net heat flux.

It is necessary to mention here that a comparison with the reanalysis datasets suggests that the ICOADS fields can provide useful information on long-term monthly means in the tropics and the southern hemisphere, north of 40ºS (Taylor, 2000). In addition, concerning NOCS, it is important to note that the field quality has strong spatial dependence reflecting the global distribution of ship observations. In particular, south of 40ºS, errors in the fields are likely to be large, and Josey et al. (1999) specifically recognize that spurious features are generated during the objective analysis of the original raw fields, as was the case in the previous Original SOC Flux Climatology. Therefore, for the southern Pacific, the region under consideration was limited to latitudes north of 40ºS.

In the region under study (to validate the dataset), we ensured that annual averages of net heat flux uncertainties off the coast did not exceed 13 W m^{-2} (Fig. 1(b)).

The meteorological variables used were: SST; total cloud amount (TCA); sea level pressure (SLP); 10 m stability dependent air temperature (AST); 10 m air specific humidity; and 10 m stability dependent wind speed (WS). 10 m stability dependent means that their estimates have been

adjusted to a standard level of 10 m above sea level using the wind profile relationship of Smith (1980). Additionally, we computed the air–sea specific humidity difference (Δq) as the difference between the air (q_a) and the sea surface (q_s, where specific humidity is assumed to be at 98 per cent saturation at SST). Δq was calculated considering the specific humidity at saturation based on Teten's formula for saturation vapor pressure from Buck (1981).

Simple Ocean Data Assimilation (SODA)

We used monthly mean temperatures from the surface (5 m) to approximately 600 m (twenty vertical levels) from the SODA reanalysis (Version 2.0.2–4) of ocean climate variability (Carton et al. 2000) onto a uniform 0.5˚ spatial grid. SODA is an ocean reanalysis product that combines observations (historical archive of hydrographical profiles supplemented by ship intake measurements, moored hydrographical observations, and remotely sensed SST and sea level) with a general ocean circulation model (Geophysical Fluid Dynamics Laboratory MOM2 physics). Surface wind forcing for SODA2.0.2–4 is provided by the recent European Centre for Medium Range Weather Forecasts ERA-40 reanalysis. SODA utilizes a multivariate sequential data assimilation scheme in which observations of ocean temperature and salinity are used to update the ocean model. More details are provided by Carton and Giese (2008).

Gridded monthly mean temperature profiles from SODA output were used to calculate the monthly mean mixed layer depth (MLD). To compute the MLD, we used the criterion based on the shallowest extreme curvature of the near surface layer temperature profiles (Lorbacher et al. 2006). These profiles show that when using historical global hydrographic profile data, this criterion is more reliable than the Δ-criterion (the depth where the quasi-homogeneous profile of temperature has decreased from the reference value, most commonly the surface value). The computed MLD was linearly interpolated to a horizontal 1º x 1º resolution.

SeaWiFS

Monthly mean climatologies (1998–2005) of the vertical attenuation coefficient, K_{490} (the vertical attenuation coefficient for downward irradiance at 490 nm), with a horizontal resolution of 4 km, were obtained from the Sea-viewing Wide Field-of-view Sensor (SeaWiFS) (McClain et al. 2002, 2004). K_{490} describes the rate of change of Ed_{490} (downward irradiance at 490 nm) with depth (Kirk 1994) and is also commonly known as the extinction coefficient. However, up to now, the most common approach for obtaining the extinction coefficient has been by deriving its value from standard water types, which are constant in time and space, as classified by Jerlov (1976). Jerlov water types have been broadly used in oceanic modeling and heat balance studies of the mixed layer (e.g. Foltz et al. 2003; Wang and McPhaden 1999). Here, we chose to use the vertical attenuation coefficient K_{490}. This is due to its availability and well-established use for estimating the radiative flux that penetrates through the mixed layer in a large part of our study area, the eastern tropical Pacific, and the tropical Atlantic (Enfield and Lee 2005; Lee et al. 2005).

To smooth data spikes, a spatial central moving average filter, including six intervals on each side (roughly 50 km) of the central point (latitude and longitude), was applied to each monthly mean climatology. Finally, it was linearly interpolated to a horizontal 1º x 1º resolution.

Methodology and theory

In order to explain the seasonal surface heat flux climatology, we analyze the climatologies of oceanic and meteorological variables. Furthermore, to evaluate the changes occurring during ENSO events we rely on Trenberth's definition (Trenberth 1997). According to this definition, there were seven El Niño and five La Niña events during in the period of analysis, 1980–2005 (Table 1). This includes the two strongest El Niño events (1982–83, 1997–98) on record and the longest (but moderate) La Niña event (1998–2000). This time period, considering the number of El Niño events (relative to the rest of the century), is exceptional (Trenberth et al. 2007). Therefore, along with constructing a global climatology for 1980–2005, we also computed those corresponding to El Niño and La Niña events, and then their respective anomalies.

The equations explaining and describing relationships between the fluxes that incorporate the net heat flux, along with those used generally to explain SST changes within the heat budget, are presented below (Eqns 1–9). We assume that temperatures are nearly vertically uniformly distributed at the MLD that was calculated.

$$Q_t = \rho_s C_p H_{mix} \frac{\partial SST}{\partial t}, \quad \text{... 1}$$

$$H_{mix} = \frac{H_{myear} H_{mmonthly}}{(H_{myear} + 1.5 H_{mmonthly\ center})}, \quad \text{... 2}$$

$$Q_{sw} = (1-\alpha) Q_C (1 - 0.62n + 0.0019\theta_n), \quad \text{... 3}$$

$$Q_{lw} = \varepsilon\sigma\, SST^4 (0.39 - 0.05e^{1/2})(1 - \lambda n^2) + 4\varepsilon\sigma\, SST^3 (SST - AST), \quad \text{... 4}$$

$$Q_{lat} = \rho_a L C_{lat} u (q_s - q_a), \quad \text{... 5}$$

$$Q_{sen} = \rho_a c_p C_{sen} u (SST - AST), \quad \text{... 6}$$

$$Q_{net} = Q_{sw} + Q_{lw} + Q_{lat} + Q_{sen}, \quad \text{... 7}$$

$$Q_{pen} = -0.45 Q_{sw} e^{-\gamma H_{mmonthly}}, \quad \text{... 8}$$

$$Q_t = Q_{net} + Q_{pen} + Q_{res} \quad \text{... 9}$$

Table 1. ENSO events (year/month) according to Trenberth's definition (Trenberth, 1997)

El Niño events	*La Niña events*
1982/05-1983/06	1984/10-1985/09
1986/09-1988/02	1988/05-1989/05
1991/05-1992/07	1995/09-1996/03
1994/07-1995/03	1998/07-2000/06
1997/05-1998/04	2000/10-2001/02
2002/05-2003/03	
2004/07-2005/02	

When the ocean gains (loses) heat, the surface flux terms are positive (negative). Eqn 1 is derived from the MIX_{season} model by Dommenget (2000), and does not consider horizontal mixing. This model is seasonally dependent on the MLD version (H_{mix}). Dommenget (2000) derived H_{mix}, using the 50-year monthly mean values for the MLD (a two-layer model), which basically follows the Levitus (1982) climatology. In the mid-latitudes, the depth of the mixed layer follows a pronounced seasonal cycle (de Boyer Montégut et al. 2004). According to Eqn 1, a change in the H_{mix} must have an effect on SST variability. The seasonal cycle of H_{mix} was determined by Eqn 2 considering the computation of monthly mean MLD. In Eqn 1, Q_t is the rate of heat storage; ρ_s is seawater density, 1022.4 kg m^{-3} and C_p is heat capacity, 3940 J kg^{-1} ºC^{-1}. In Eqn 1, we estimate Q_t using differences centered in time. In Eqn 2, H_{myear} is the annual mean isothermal layer depth and $H_{mmonthly}$ is the monthly mean MLD. $H_{mmonthly\ center}$ is the center (half) of the monthly mean MLD. The factor 1.5 for $H_{mmonthly\ center}$ has been introduced to somewhat reduce the MLD in the MIX_{season} model.

The air–sea fluxes obtained from NOCS v2.0 use bulk formulas from Smith (1988) for turbulent fluxes, Reed (1977) for the net shortwave flux, and Clarke et al. (1974) for the net longwave flux (Eqns 3–6). Here, Q_{sw} is the shortwave solar radiation that enters the mixed layer; Q_{lw} is the outgoing longwave radiation; Q_{lat} is the latent heat flux; Q_{sen} is the sensible heat flux; Q_c is the clear-sky solar radiation; n is the daily mean fractional cloud cover; θ_N is the local noon solar elevation; α is the albedo of the sea surface; ε is the emittance of the sea surface; σ is the Stefan–Boltzmann constant; e is the water vapor pressure; λ is a latitude-dependent cloud cover coefficient; ρ_a is the density of air; c_p is the specific heat capacity of air at constant pressure; L is the latent heat of vaporization; C_{lat} and C_{sen} are the stability- and height-dependent transfer coefficients for latent and sensible heat, respectively; u, AST and q_a are the scalar wind speed, air temperature, and air specific humidity at 10 m, respectively; and q_s is 98 per cent of the saturation specific humidity at SST. The sum of the four terms in Eqn 7 is the net surface heat flux across the air–sea interface, Q_{net}.

The shortwave radiation that penetrates through the base of the mixed layer, Q_{pen}, was estimated by applying Eqn 8, where the extinction coefficient γ is K_{490}. Advection and diffusion are treated as residuals (Q_{res}). To see if the SST ($\partial SST/\partial t$) tendency is related to the heat budget terms, we compared it with the sum of $Q_{net} + Q_{pen}$. This relationship would be similar if residuals and errors in the heat fluxes were negligible. In summary, we obtained the air–sea fluxes from NOCS v2.0, computed Q_{pen} and Q_t.

Results and Discussion

We present the seasonal and interannual analysis of the most important components of the surface heat fluxes and the relationship of $Q_{net} + Q_{pen}$ and SST tendency.

Seasonal timescales

Radiative fluxes

Q_{sw}

The annual mean cloud cover structure is divided roughly into two main regions, 70%±15% over 10ºN–25ºS, and 60%±7% over 25ºS–40ºS (Fig. 3(a)). North of 25ºS, TCA (total cloud amount) presents a seasonal cycle with values that are greater over the latter half of the year than during the first half. This reduces the amount of shortwave energy, particularly over the northeastern equatorial Pacific by roughly twenty per cent, as already noted by Wang and McPhaden (2001a). The higher amount of cloud cover north of 5°N is associated with the presence of the ITCZ (Garcés-Vargas et al. 2004; Waliser and Gautier 1993). In contrast, the equatorial area and southeast Pacific to about 30°S, are associated with a greater frequency of low stratocumulus (Norris 1998). Note that the TCA does follow a seasonal cycle over the equator, despite the lack of a solar seasonal cycle at these latitudes. South of 25ºS, it reaches its peak during the June–August.

Thus, the pattern of Q_{sw} is influenced by both the annual mean and seasonal difference distribution in the solar latitudinal position and TCA (Fig. 4(a)). As a result, the annual mean values of Q_{sw} decrease gradually to the south, while the seasonal variance increases inversely (210±30 W m^{-2} over 10ºN to the equator, 200±50 W m^{-2} over the equator to 15ºS, 180±70 W m^{-2} over 15ºS–30ºS and 160±110 W m^{-2} at 40ºS) (Fig. 4(a)). North of the equator, Q_{sw} shows a double peak, during the austral/boreal summer according to the twice per year passage over the equator. Nevertheless, the greatest values of Q_{sw} take place during the austral summer, the second peak reduced by the greater amount of cloud. South of the equator too, at 5ºS–25ºS, the highest values of TCA, occurring during the latter half of the year, significantly reduce Q_{sw}. At 30ºS–35ºS, the highest values of TCA, which occur during July and August, imply minima of about 100 W m2, while during spring, the lowest TCA values give rise to maxima (beyond 200 W m^{-2}).

Q_{lw}

Generally, Q_{lw} (Fig. 4(b)) follows the shape of the TCA (Fig. 3(a)). The annual mean values of Q_{lw} release less heat to the north of the equator to 10ºN around –35 (±15) W m^{-2}, south of the equator to 25ºS about –45 (±5) W m^{-2} and south of 25ºS roughly –55 (±10) W m^{-2}. In the northern region, the main release takes place during December–April, and less so during the rest of the year. From 5ºS–15ºS and 15ºS–25ºS, there is a slightly greater release during March–June and January–April, respectively. South of 25ºS, there is greater release from 33ºS–37ºS attaining –65 W m^{-2} during September–November.

The greater cloudiness during the second half of the year in the first two regions allows a smaller amount of heat released by Q_{lw}, especially in the first region (10°N to the equator). South of 30ºS, a relatively narrow seasonality of cloudiness is mainly associated with the influence of the southern coastal jet. This allows greater heat release by Q_{lw} at these latitudes (over the first two regions) as suggested by Renault et al. (2009), who analyzed the impact of this coastal jet on SST. This is also similar to what has been observed west of the eastern Pacific coast (Cronin et al. 2006b).

Therefore, as a summary of the radiative fluxes, Q_{sw} follows the change in cloud cover and sun position with latitude, while Q_{lw} roughly follows the former. Unlike Q_{sw}, the Q_{lw} varies little year round and presents average values of 1/3 (10ºN to the equator) to 1/5 (30ºS–40ºS) of Q_{sw} values. As a result, Q_{sw} displays strong seasonality, while Q_{lw} fluctuates over a narrow band. Therefore, the seasonal variability of the radiative fluxes is well represented by Q_{sw}.

Turbulent fluxes

Q_{lat}

Q_{lat} patterns follow those of Δq (negative, varying from –1 to –6 x 10^{-3} kg kg^{-1}) multiplied by the wind speed magnitude (WS, varying from 4 to 9 m s^{-1}) (Eqn 5).

The structure of WS and Δq is roughly equally divided into four main regions, 4–6 m s^{-1} (10ºN to the equator), 4–7 m s^{-1} (equator to 15ºS), 5–6 m s^{-1} (15ºS–25ºS), 7–9 m s^{-1} (25ºS–40ºS) (Fig. 3(b)). For Δq, mean values are –4/–6, –3.5/–2, –4.5/–3.5, and –2/–1 x 10^{-3} kg kg^{-1}, respectively (Fig. 3(c)). Thus, Q_{lat} presents roughly the same regional structure: 10ºN to the equator, around –80±30 W m^{-2}; equator to 15ºS, –65±20 W m^{-2}; 15ºS –30ºS, –70±20 W m^{-2}; 30ºS–40ºS, –60±10 W m^{-2} (Fig. 4(c)).

However, WS and Δq do not distribute their seasonal cycle equivalently. For WS, a seasonal cycle is only clearly evident at the equator to 15ºS (highest/lowest WS occurs during austral winter/summer [Fig. 3(b)]) and at 25ºS–40ºS (highest WS takes place at the end of austral spring/mid-summer). For Δq, a contrast between the first and the latter half of the year occurs in all regions studied (10ºN–40ºS) (Fig. 3(c)). For 10ºN–2ºS and 30ºS–40ºS, Δq peaks during the austral autumn, with a minimum during the austral spring. For 2ºS–30ºS, it is exactly the reverse.

As a result, the seasonal amplitude of Q_{lat} (Fig. 4(c)) is principally related to that of Δq, but its magnitude is attenuated thanks to WS. Let us note that Jiang et al. (2005), using TAO buoy measurements along the tropical Pacific and different state variables from different atmospheric reanalyses, presented similar results. Their error analysis also suggests that Q_{lat} changes are principally driven by Δq. Thus, north of 2ºS, heat is released over the second part of the year, where it reaches up to –125 W m^{-2} at 2ºN (Fig. 4(c)).

Fig. 3. Latitude–time plot climatology with its respective zonal mean (red line) and range (blue dash-dot lines) of the air–sea variables alongshore the coast (~200 km). (a) Total cloud amount (TCA [%]), (b) wind speed (WS [m s^{-1}]), (c) air–sea specific humidity difference (Δq [kg kg^{-1}]), and (d) mixed layer depth (MLD [m]). Month number is shown on bottom axis of the left-hand side of each panel. The right-hand colour bar in each latitude–time plot displayed applies.

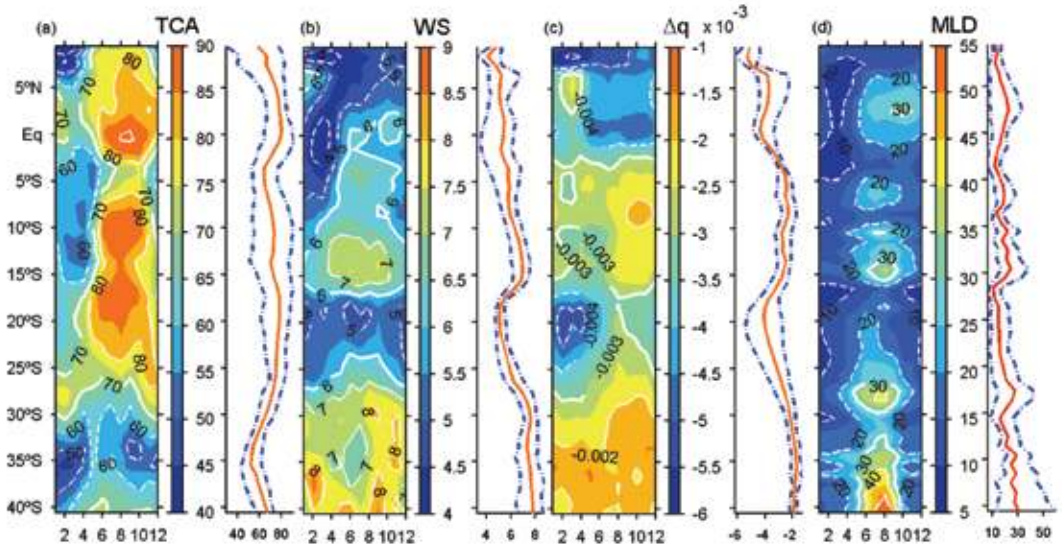

From roughly 2ºS to 10ºS, heat is released slightly due to the relatively slight Δq (despite strong winds). Conversely, heat is released over the first half of the year from 10ºS to 30ºS, with the greatest release at 20ºS–25ºS peaking in March (Fig. 4(c)). According to the structure of Δq and the seasonal wind magnitude, south of 30ºS, Q_{lat} values are small and no clear seasonal cycle emerges.

Q_{sen}

Q_{sen} presents an equivalent structure to ΔST (SST–AST) (figures not shown), agreeing with the error analysis of Jiang et al. (2005), but it does not present an important seasonal variability compared to Q_{lat} (the least important of all the fluxes studied here). Thus, the variability of the turbulent fluxes is well represented by Q_{lat} alone, similar to what is found in the eastern Pacific (Colbo and Weller 2007; Cronin and McPhaden 2001; Cronin et al. 2006a; McPhaden et al. 2008; Wang and McPhaden 1999).

The variability of turbulent fluxes is indeed related to seasonal climate variability along these regions. Thus, during the austral summer, when the southeast trade winds are weak and the ITCZ is located at its most southern position (Garcés-Vargas et al. 2004; Waliser and Gautier 1993), the cyclonic eddy induced by the Panama wind jet results in Ekman suction and reduces SST (Rodríguez-Rubio and Stuardo 2002; Rodríguez-Rubio et al. 2003). This causes a decrease in heat released by Q_{sen} and Q_{lat} due to a reduction in Δq and ΔST, respectively. By contrast, during the austral winter, southeast trade winds are strong and the ITCZ is located at its most northern position (Garcés-Vargas et al. 2004; Waliser and Gautier 1993), preventing the passage of the Panama wind jet. This tends to increase the surface temperature and increase Δq and ΔST, therefore producing an increase in the heat released by Q_{sen} and Q_{lat}, respectively.

South of the equator, the major releases to the atmosphere and seasonal variations by Q_{lat} occur between 15ºS and 30 ºS. In this area, Δq has high values and large seasonal variability. However, the winds are weak and constant; in this sector the influence of the southeast Pacific anticyclone is quasi-permanent (Montecino et al. 2006). On the other hand, south of 30ºS, the influence of the coastal jet induces a slight heat release and small range of seasonal variability associated with Q_{lat}. In this zone, the winds are strong throughout the year, while Δq remains low.

Q_{net}

Given the variance of the different participating heat fluxes, larger for the radiative than for the turbulent fluxes ($Q_{rad} > Q_{tur}$), Q_{net} will preferentially represent Q_{rad} (Fig. 4(d)). Within the radiative fluxes, Q_{sw} has the largest variance, while Q_{lat} has the largest variance among the turbulent fluxes. As a result, the seasonal variance of Q_{net} will occur primarily from the balance between the heat storage due to Q_{sw} and the heat release by Q_{lat}.

However, Q_{sw} is significantly higher than Q_{lat} (two to four times higher). Therefore, Q_{net} has the shape of Q_{sw}. This is similar to what has been found elsewhere: e.g. over the eastern equatorial Pacific (Cronin et al. 2006a; McPhaden et al. 2008; Wang and McPhaden 1999, 2001a) or the tropical Atlantic (Foltz et al. 2003).

We note that what influences Q_{net} the most is precisely its seasonal variance. From north to south, the seasonal variability of Q_{net} has negative values over the austral winter from 10ºS to 40ºS. It varies from about –20 W m^{-2} at 10ºS–20ºS to –30 W m^{-2} at 20ºS–30ºS and around –40 to –60 W m^{-2} at 30ºS–40ºS (Fig. 4(d)). Given the regional structure of Q_{lat}, it will drop further between 10ºN and the equator, preferentially during the latter half of the year (100–150 W m^{-2}), and at 15ºS–30ºS during the first half of the year (> 80W m^{-2}). Comparisons with the mean annual cycle of Q_{net} at 95°W and 8°S–10ºN from TAO/EPIC buoy measurements by Cronin et al. (2006a) and McPhaden et al. (2008) show similarities in the pattern but with a spatial difference of about two degrees according to the location of the equatorial front, which is further south close to the coast (Fig. 1). Those differences arise mainly from Q_{lat}.

Fig. 4. Latitude–time plot climatology with its respective zonal mean (red line) and range (blue dash-dot lines) of the heat fluxes alongshore the coast (~200 km). (a) Shortwave solar radiation (Q_{sw}), (b) outgoing longwave radiation (Q_{lw}), (c) latent heat flux (Q_{lat}), (d) net surface heat flux (Q_{net}), (e) shortwave radiation that penetrates through the base of the mixed layer (Q_{pen}), (f) $Q_{net} + Q_{pen}$, and (g) SST tendency ($\delta SST/\delta t$). Month number is shown on bottom axis of the left-hand side of each panel. The heat flux scale (W m^{-2}) and SST tendency (ºC month^{-1}) is displayed in (a) to (f) and (g) respectively, to the right of each latitude–time plot.

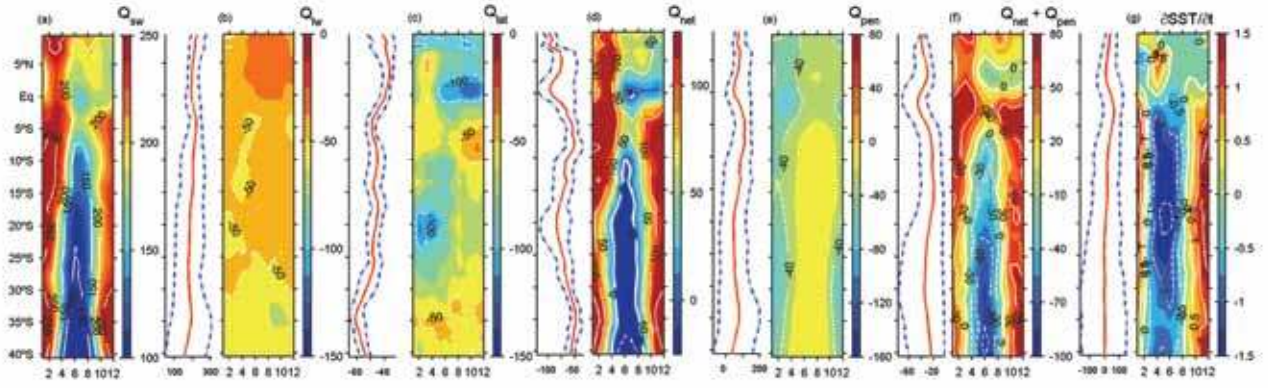

We also note that below 10°S, Q_{net} represents a gain for the ocean, similar to what has been observed in the eastern equatorial Pacific and Atlantic (Berry and Kent 2009). Even at southern latitudes, a minor incoming Q_{sw} during the winter months (even during the autumn south of 20°S) allows the ocean to release heat by Q_{net}. This is similar to what has been observed at a buoy located at 20ºS, 85ºW (Colbo and Weller 2007).

However, it is not possible to omit the role of the sum of Q_{lw} and Q_{sen} as it increases the annual mean heat released and it varies from north to south. Thus, along with Q_{lat} (Fig. 4(c)), the contributions of Q_{sen} and Q_{lw} increase the annual mean heat released to the atmosphere by about 110±20 W m^{-2} along most of the latitudes analyzed here. As a result, the latitudinal evolution of the annual mean heat storage by Q_{sw} is balanced by the heat released by the different processes involved (annual mean contributions by Q_{lat}, Q_{sen} and Q_{lw}).

De Szoeke et al. (2010) found that three different observation-based gridded flux products (NCAR CORE, WHOI OAFlux, and UW Hybrid) agree well with ship transect (along 20ºS from 75ºW to 85ºW) and buoy (20ºS, 85ºW) observations during the austral spring, interestingly, especially in a region where climate models are known to exhibit errors. Thus, in order to test the quality of the gridded fluxes used here, and therefore our results, one of the products used by de Szoeke et al. (2010) was chosen: the OAFlux dataset (Yu and Weller 2007). Along the EPC investigated here, the largest differences between both datasets in Q_{net} are found between the equator and 10°S. This takes place mainly during the austral winter and is associated with differences in Q_{lat} and Q_{lw} of about 30 W m^{-2} and 40 W m^{-2}, respectively. However, this is precisely the region in which the NOCS dataset presents fewer uncertainties (Fig. 1) (compared to those of OAFlux). The OAFlux dataset might present problems near the coastal regions where the satellite sensors have problems to retrieving data. Differences at other latitudes were low, of about ± 20 W m^{-2} for Q_{net}. As a result, we believe that within the region investigated here, the NOCS fluxes are at least as good as other datasets.

The shortwave radiation that penetrates through the base of the mixed layer (Q_{pen})

Q_{pen} is always lost heat; therefore, it is a negative term. To some extent, Q_{pen} mirrors Q_{sw}, although it presents differences that the MLD and the extinction coefficient modulate. Therefore, we will describe briefly the variations of MLD before discussing Q_{pen}.

The annual mean of MLD varies slightly with latitude. It is about 15 m north of the equator, 18 m between the equator and 15ºS, and about 12 m from 15–20ºS, and then it increases to 25 m south of 20ºS (Fig. 3(d)). Again, the seasonal variance is particularly striking south of the equator: between 5ºN and the equator (± 10 m), 10ºS–15ºS (±15m), 25ºS–30ºS (± 15 m) and south of 35ºS (±25 m). The MLD presents its peak during the austral winter south of 5ºS and during spring to the north. As a result, given Q_{sw} and MLD, the heat lost by Q_{pen} is less during winter and greater in summer (less than 20 W m^{-2} on average). Consequently, more heat is lost where the MLD is shallower: i.e. during the spring–summer over 15ºS–30ºS (about 40–80 W m^{-2}) and during the end of summer through to autumn north of 5ºS (40–60 W m^{-2}) (Fig. 4(e)). This is similar to what has been reported by Wang and McPhaden (1999) and McPhaden et al. (2008) for the TAO moorings in the eastern equatorial Pacific. Finally, compared with Q_{net}, Q_{pen} is nearly three times smaller.

Q_{net} + Q_{pen} comparison with SST tendency

The SST tendency has to be related to different heat budget terms that give rise to changes in SST. Therefore, it is possible to shed some light on these while comparing the SST tendency with the sum of Q_{net} + Q_{pen}.

Over roughly 10ºN–2ºN, the sum Q_{net} + Q_{pen} shows less heat gain in spring–summer (Fig. 4(f)). These results stress the importance of Ekman suction produced by the Panama wind jet that induces upwelling, which tends to cool the mixed layer (SST) (Devis-Morales et al. 2008). Within equatorial waters (2ºN–5ºS), Q_{net} + Q_{pen} shows a heat gain throughout the year with the minima during the austral winter. However, an increase in SST is only just evident at the beginning and end of the year (Fig. 4(g)). This could be explained principally by the presence of year-round equatorial upwelling (Fiedler, 1992; Pennington et al. 2006).

The SST patterns between 10ºS and 35ºS show greater cooling in winter than for Q_{net} + Q_{pen} (Fig. 4(f)). Therefore, the role of the Ekman transport over the Eastern Boundary Current Peru/Chile tends to cool the mixed layer (SST) (Croquette et al. 2007; Soto-Mardones et al. 2004; Takahashi 2005) and on average leads to higher upwelling than Ekman pumping (Croquette et al. 2007). Further south, warming of SST is only evident during spring–summer but with less intensity than Q_{net} + Q_{pen} (Fig. 4(g)). This could be explained by the coastal upwelling that occurs during these seasons (Sobarzo et al. 2007) and coincides with the influence of wind-driven upwelling/entrainment off central Chile on SST fluctuations (Hormazabal et al. 2001).

Other oceanic terms must also be considered. For example, the interplay of advective and diffusive terms may play a role along the north of the equator (Chaigneau et al. 2006) and the Humboldt Current system may also be important (Bravo 2003; Chaigneau and Pizarro 2005; Hormazabal et al. 2001).

Interannual timescales

Radiative fluxes

It is well known that the ENSO warm phase is connected with the weakening of the subtropical anticyclone and the southern migration of the ITCZ, and inversely during the cold phase (Rutllant 2004). Therefore, we would expect changes in radiative fluxes. During ENSO events, TCA values change only a little with respect to their climatology (less than twenty per cent, figure not shown). Given this small TCA

variability, and as Q_{lw} and Q_{sw} have opposite relationships to the ENSO phase, this gives rise to Q_{sw} changes of about 10–15 W m^{-2} (negative during El Niño, positive during La Niña) and opposite anomalies in the order of 5–10 W m^{-2} in Q_{lw}. Therefore, Q_{lw} and Q_{sw} counterbalance each other as also observed in the eastern equatorial Pacific (Liu and Gautier 1990; Wang and McPhaden 2000, 2001b; Yu and Weller 2007). Thus, positive anomalies of radiative fluxes occur during El Niño, and inversely so during La Niña (figures not shown).

Turbulent fluxes

At interannual timescales, ENSO changes are associated with Q_{lat}, which are related to both wind and Δq anomalies.

For El Niño, wind anomalies decrease (about 0.5 m s^{-1}) year round (excluding January–February) over 10ºN to the equator and intensify during summer–autumn for Eq–15ºS, and spring–summer for 20ºS–40ºS. Roughly, the opposite takes place during La Niña.

On the other hand, over almost all regions the Δq anomalies are largely negative (between 0.0005–0.001 kg kg^{-1}) during El Niño, and partly positive (0.0002–0.0005 kg kg^{-1}) during La Niña (Figs. 5(f) and 6(f)). Since a change in Δq does not affect variations in Q_{sen}, and Q_{lat} varies more than Q_{sen}, we expect that Bowen ratio (Q_{sen}/Q_{lat}) anomalies are mostly negative during El Niño (more heat loss by Q_{lat}) and positive during La Niña (less heat loss by Q_{lat}). The main Q_{tur} anomalies are concentrated between the equator and 15ºS and are negative for El Niño and positive for La Niña (Fig. 5(a) and 6(a)), directly related to Δq anomalies and the slight change of wind magnitudes, as has also been noted elsewhere: e.g. for the Caribbean Sea (Chikamoto and Tanimoto 2005) or the tropical Atlantic (Chikamoto and Tanimoto 2006). Thus, in this region, more heat is lost during March–April (30–50 W m^{-2}) for El Niño, and less so during May–June (20–30 W m^{-2}) for La Niña.

Q_{net}

The variance of the radiative fluxes is insignificant compared to that of the turbulent fluxes ($Q_{rad} << Q_{tur}$). Given that the interannual variability of Q_{sen} is negligible, Q_{net} reproduces almost exactly the Q_{lat} patterns, enhanced/decreased slightly by Q_{sw} (figures not shown). Greater anomalies in Q_{tur} are then concentrated between the equator and 25ºS during the first half of the year.

The shortwave radiation that penetrates through the base of the mixed layer (Q_{pen})

During the ENSO cycle, opposite patterns arise depending on the events. As the MLD and thermocline deepens during El Niño, it allows a small heat loss by Q_{pen}, mainly over 5ºS–25ºS (maximum located over 10ºS –20ºS, 20 W m^{-2}). Inversely during La Niña, a shallower MLD and thermocline induce a greater amount of heat released by Q_{pen}, particularly between the equator and 30ºS—about 20 W m^{-2}. Both cases take place mainly during the austral summer.

Interestingly, this analysis shows that north of the equator (between the equator and 10ºN), during most of the year, Q_{pen} tends to lose heat during El Niño while storing during La Niña. Along equatorial latitudes, the MLD deepens during El Niño, and becomes less deep during La Niña (Wang and McPhaden, 2000, 2001b). In this case, this is probably related to a greater ocean barrier layer thickness associated with a more stratified water column due to river runoff from western Colombia and Ecuador (Devis-Morales et al. 2008).

Q_{net} + Q_{pen} comparison with SST tendency

From the equator down to 20ºS–25ºS and within the first months of the year, Q_{net} + Q_{pen} tends to cool during El Niño and warm during La Niña (Figs. 5(c) and 6(c)). However, the SST tendency is the opposite (Figs. 5(d) and 6(d)). It is known that the eastward equatorial current anomalies occur along the tropical Pacific during El Niño and westward during La Niña (Lagerloef et al. 2003; Vialard et al. 2001), and current anomalies also spread along the coast. This process would explain most of the positive anomalies in SST during El Niño and the negative anomalies during La Niña. It appears that SST anomalies are driving the Q_{net} + Q_{pen}, which acts as a negative feedback, in line with what has already been observed in the eastern equatorial Pacific (Wang and McPhaden 2000). Like seasonal scale, other oceanic terms must also be considered.

Conclusion

We analyzed the surface heat fluxes along the eastern Pacific coast (10ºN–40ºS, ~200 km off the west coast of Central–South America) at seasonal and interannual timescales. Particularly, along with other databases, we investigated the NOCS Flux Dataset v2.0 (26 years: 1980–2005), a database which includes the recently updated air–sea heat fluxes NOC dataset. They were analyzed in detail based on their corresponding meteorological and oceanographic variables. On a seasonal scale, results show that within all the fluxes contributing to Q_{net}, Q_{sw} is the term that warmed and most dominated. The terms that most contributed to cooling were led by Q_{lat}. Q_{sw} reduction due to cloud cover during the latter half of the year was associated with the presence of the ITCZ north of the equator and the stratus cloud deck between the equator and 30ºS. The less significant seasonal range southward of 30ºS is linked to the southern coastal jet that arises along the eastern rim of the low-level circulation over the southeast Pacific high. At an interannual scale, the main change was observed for Q_{lat} during the first half of the year, between 0º and 20ºS. Q_{lat} tended to cool (warm) during the ENSO warm (cold) phase, acting as a negative feedback. Particularly for Q_{lat}, we noticed that the air–sea specific humidity difference played a major role (more than the wind) during El Niño and La Niña. Differences in the pattern of SST tendency and Q_{net} + Q_{pen} provide evidence that in some areas the advective terms are important at seasonal and interannual scale.

Fig. 5. Latitude–time plot anomalies of the surface heat fluxes and meteorological variables alongshore the coast (~200 km) during El Niño. (a) Turbulent fluxes ($Q_{lat} + Q_{sen}$), (b) shortwave radiation that penetrates through the base of the mixed layer (Q_{pen}), (c) $Q_{net} + Q_{pen}$, (d) SST tendency ($\delta SST/\delta t$), (e) sea surface temperature (SST), and (f) air–sea specific humidity difference (Δq). Month number is shown on bottom axis. The surface heat fluxes scale (W m^{-2}) is displayed to the right of $Q_{net} + Q_{pen}$. The scale of SST (ºC) and Δq (kg kg^{-1}) is displayed to the right of each panel.

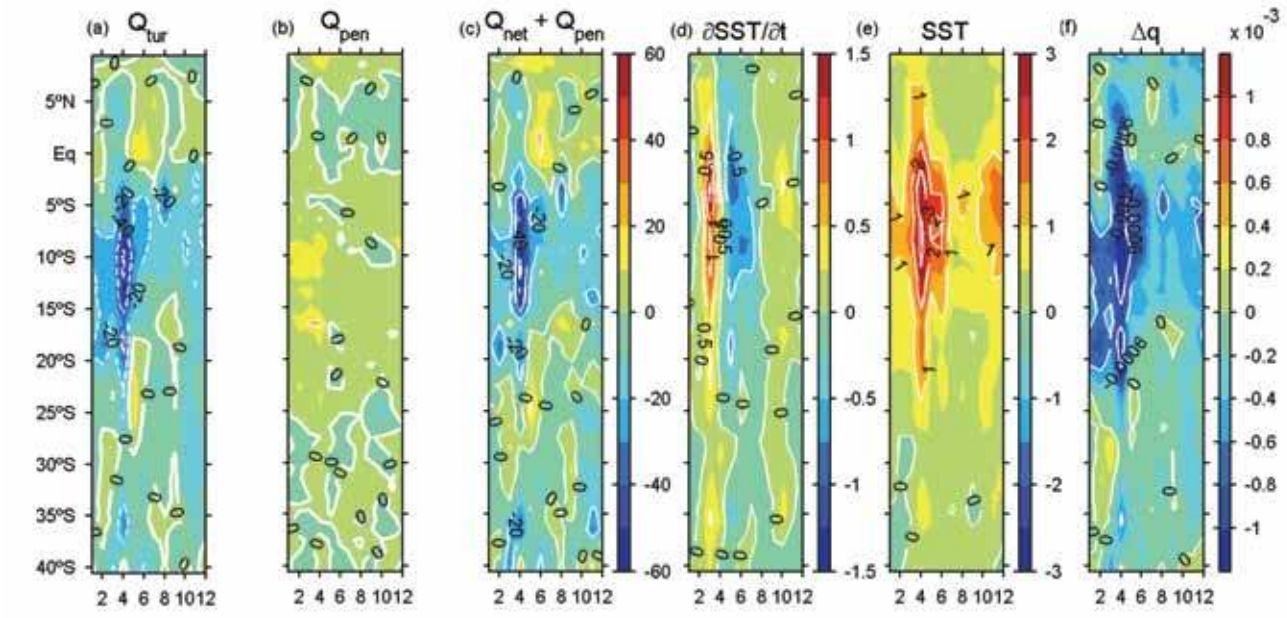

Fig. 6. Latitude–time plot anomalies of the surface heat fluxes and meteorological variables alongshore the coast (~200 km) during La Niña. (a) Turbulent fluxes ($Q_{lat} + Q_{sen}$), (b) shortwave radiation that penetrates through the base of the mixed layer (Q_{pen}), (c) $Q_{net} + Q_{pen}$, (d) SST tendency ($\delta SST/\delta t$), (e) sea surface temperature (SST), and (f) air–sea specific humidity difference (Δq). Month number is shown on bottom axis. The surface heat flux scale (W m^{-2}) is displayed to the right of $Q_{net} + Q_{pen}$. The scale of SST (ºC) and Δq (kg kg^{-1}) is displayed to the right of each panel.

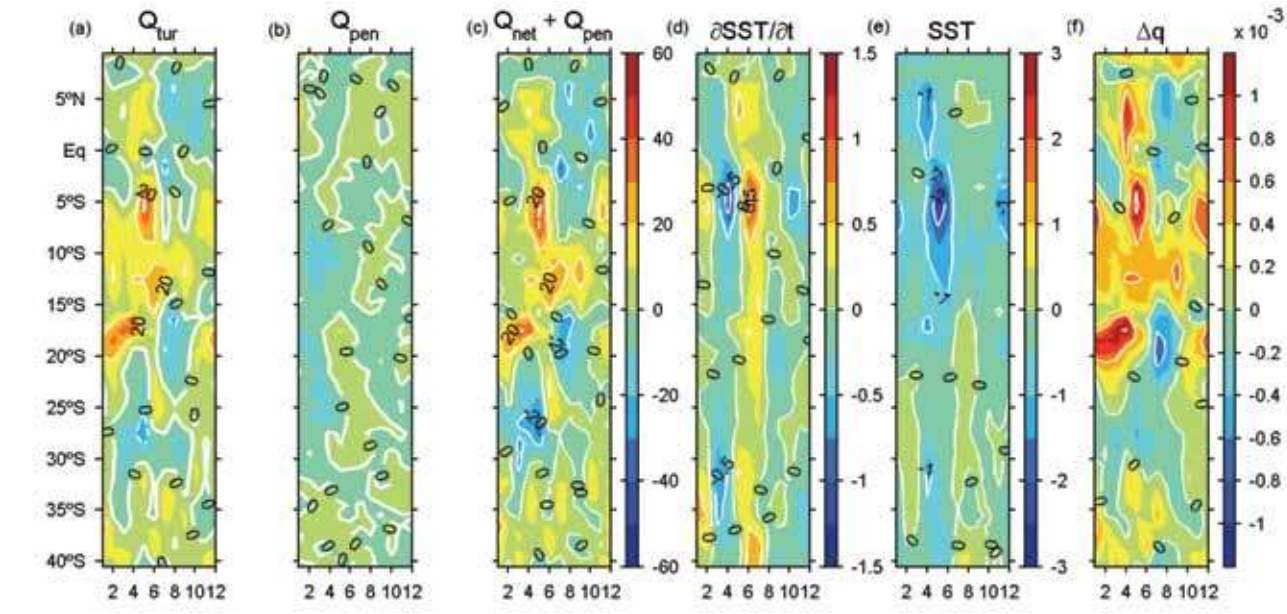

Acknowledgments

The authors would like to thank Gerard Eldin and Vincent Echevin for helpful comments on an earlier version of this manuscript. The original manuscript was substantially improved in both form and content in many ways with the help of two anonymous reviewers. We would like to thank them for their hard work. This research was supported by FONDECYT-IRD Postdoctoral program No. 3060117.

References

Amador, J.A., Alfaro, E.J., Lizano, O.G. and Magana, V.O. 2006. Atmospheric forcing of the eastern tropical Pacific: A review. *Prog. Oceanogr, 69,* 101–142.

Berry, D.I. and Kent, E.C. 2009. A New Air-Sea Interaction Gridded Dataset from ICOADS with Uncertainty Estimates. *Bull. Amer. Meteorol. Soc., 90,* 645–656.

Berry, D.I. and Kent, E.C. 2011. Air-Sea fluxes from ICOADS: the construction of a new gridded dataset with uncertainty estimates. *Int. J. Climatol., 31,* 987–1001.

Borovikov, A., Rienecker, M.M. and Schopf, P.S. 2001. Surface Heat Balance in the Equatorial Pacific Ocean: Climatology and the Warming Event of 1994–95. *J. Clim., 14,* 2624–2641.

Bravo, L. 2003. Variabilidad anual e interanual de la profundidad de la capa de mezcla y de la termoclina en la zona norte de Chile (18°20ºS - 24ºS), Undergraduate, Escuela de Ciencias del Mar, Pontificia Universidad Católica de Valparaiso.

Buck, A.L. 1981. New equations for computing vapor pressure and enhancement factor. *Journal Appl. Meteorol., 20,* 1527–1532.

Carton, J.A. and Giese, B.S. 2008. A reanalysis of ocean climate using Simple Ocean Data Assimilation (SODA). *Mon. Wea. Rev., 136,* 2999–3017.

Carton, J.A., Chepurin, G., Cao, X.H. and Giese, B. 2000. A Simple Ocean Data Assimilation analysis of the global upper ocean 1950-95. Part I: Methodology. *J. Phys. Oceanogr., 30,* 294–309.

Caviedes, C. 2000. ENSO in South America (Chapter 3). *El Niño-Southern Oscillation and its Global Impacts.* L. C. Nkemdirim, Ed., 256.

Clarke, N.E., Eber, L., Laurs, R.M., Renner, J.A. and Saur, J.F. 1974. *Heat exchange between ocean and atmosphere in the eastern North Pacific for 1961-71.* 108 pp.

Colbo, K. and Weller, R. 2007. The variability and heat budget of the upper ocean under the Chile-Peru stratus. *J. Mar. Res., 65,* 607–637.

Cronin, M.F. and McPhaden, M.J. 2001. Surface heat fluxes from the TAO Enhanced Array along 95ºW. *WCRP/SCOR Workshop on Intercomparison and Validation of Ocean-Atmosphere Flux Fields,* Washington DC, WMO/TD-No. 1083,

Cronin, M.F. and Sprintall, J. 2001. Wind and Buoyancy-Forced Upper Ocean. *Encyclopedia of Ocean Science.* J. Steele, S. Thorpe and K. Turekian, Eds., 3219–3227.

Cronin, M.F., Fairall, C.W. and McPhaden, M.J. 2006a. An assessment of buoy-derived and numerical weather prediction surface heat fluxes in the tropical Pacific. *J. Geophys. Res., 111,* doi:10.1029/2005JC003324.

Cronin, M.F., Bond, N.A., Fairall, C.W. and Weller, R.A. 2006b. Surface cloud forcing in the East Pacific stratus deck/cold tongue/ITCZ complex, *J. Clim., 19,* 392–409.

Croquette, M., Eldin, G., Grados, C. and Tamayo, M. 2007. On differences in satellite wind products and their effects in estimating coastal upwelling processes in the south-east Pacific. *Geophys. Res. Lett., 34,* L11608, doi:10.1029/2006GL027538.

Chaigneau, A. and Pizarro, O. 2005. Mean surface circulation and mesoscale turbulent flow characteristics in the eastern South Pacific from satellite tracked drifters. *J. Geophys. Res., 110,* doi:10.1029/2004JC002628.

Chaigneau, A., Abarca del Rio, R. and Colas, F. 2006. Lagrangian study of the Panama Bight and surrounding regions. *J. Geophys. Res., 111,* doi:10.1029/2006JC003530.

Chikamoto, Y. and Tanimoto, Y. 2005. Role of specific humidity anomalies in Caribbean SST response to ENSO. *J. Meteorol. Soc. Jpn, 83,* 959–975.

Chikamoto, Y. and Tanimoto, Y. 2006. Air-sea humidity effects on the generation of tropical Atlantic SST anomalies during the ENSO events. *Geophys. Res. Lett., 33,* doi:10.1029/2006GL027238.

de Boyer Montégut, C., Madec, G.. Fischer, A.S., Lazar, A. and Iudicone, D. 2004. Mixed layer depth over the global ocean: An examination of profile data and a profile-based climatology. *J. Geophys. Res., 109,* doi:10.1029/2004JC002378.

de Szoeke, S.P., Fairall, C.W., Wolfe, D.E., Bariteau, L. and Zuidema, P. 2010. Surface Flux Observations on the Southeastern Tropical Pacific Ocean and Attribution of SST Errors in Coupled Ocean-Atmosphere Models. *J. Clim., 23,* 4152–4174.

Devis-Morales, A., Schneider, W., Montoya-Sanchez, R.A. and Rodriguez-Rubio, E. 2008. Monsoon-like winds reverse oceanic circulation in the Panama Bight. *Geophys. Res. Lett., 35,* doi:10.1029/2008GL035172.

Dobson, F. W. and Smith, S.D. 1985. Estimation of solar radiation at sea. *The Ocean Surface.* Y. Toba and H. D. Mitsuyasu, Eds., 525–533.

Dommenget, D. 2000. Large-scale SST variability in the midlatitudes and in the tropical Atlantic, PhD., Max-Planck-Institute for Meteorology, Univertsity of Hamburg.

Enfield, D.B. and Lee, S.K. 2005. The heat balance of the Western Hemisphere warm pool. *J. Clim., 18,* 2662–2681.

Fairall, C.W., Uttal, T., Hazen, D., Hare, J., Cronin, M.F., Bond, N. and Veron, D.E. 2008. Observations of cloud, radiation, and surface forcing in the equatorial eastern Pacific. *J. Clim., 21,* 655–673.

Fiedler, P.C. 1992. Seasonal climatologies and variability of eastern tropical Pacific surface waters, U.S. Dept. of Commerce, National Oceanic and Atmospheric Administration, Seattle, 65 pp.

Foltz, G.R., Grodsky, S.A., Carton, J.A. and McPhaden, M.J. 2003. Seasonal mixed layer heat budget of the tropical Atlantic Ocean . *J. Geophys. Res., 108,* doi:10.1029/2002JC001584.

Garcés-Vargas, J., Abarca del Rio, R. and Schneider, W. 2004. Climatology and interannual variability of Intertropical Convergence Zone in the eastern Pacific. PORSEC, Concepción, Chile, Gayana, 215–217.

Garreaud, R.D. and Muñoz, R.C. 2005. The low-level jet off the west coast of subtropical South America: Structure and variability. *Mon.Wea. Rev., 133,* 2246–2261.

Ghate, V.P., Albrecht, B.A., Fairall, C.W. and Weller, R.A. 2009. Climatology of Surface Meteorology, Surface Fluxes, Cloud Fraction, and Radiative Forcing over the Southeast Pacific from Buoy Observations. *J. Clim., 22,* 5527–5540.

Hormazabal, S., Shaffer, G., Letelier, J. and Ulloa, O. 2001. Local and remote forcing of sea surface temperature in the coastal upwelling system off Chile. *J. Geophys. Res., 106,* 16657–16671.

Jerlov, N.G. 1976. *Marine Optics.* Elsevier Scientific Publishing Company, Amsterdam, 231 pp.

Jiang, C.L., Cronin, M.F., Kelly, K.A. and Thompson, L. 2005. Evaluation of a hybrid satellite- and NWP-based turbulent heat flux product using Tropical Atmosphere-Ocean (TAO) buoys. *J. Geophys. Res., 110,* C09007, doi:10.1029/2004JC002824.

Josey, S.A., Kent, E.C. and Taylor, P.K. 1998. The Southampton Oceanography Centre (SOC) Ocean-Atmosphere Heat, Momentum and Freshwater Flux Atlas. *Report No 6,* 30 pp.

Josey, S.A., Kent, E.C. and Taylor, P.K. 1999. New insights into the ocean heat budget closure problem from analysis of the SOC air-sea flux climatology. *J. Clim., 12,* 2856–2880.

Kessler, W.S. 2006. The circulation of the eastern tropical Pacific: A review, *Prog. Oceanogr., 69,* 181–217.

Kessler, W.S., Rothstein, L.M. and Chen, D. 1998. The Annual Cycle of SST in the Eastern Tropical Pacific, Diagnosed in an Ocean GCM. *J. Clim., 11,* 777–799.

Kirk, J.T.O. 1994. *Light and photosynthesis in aquatic ecosystems.* Cambridge University Press, New York, 509 pp.

Lagerloef, G.S.E., Lukas, R., Bonjean, F., Gunn, J.T., Mitchum, G.T., Bourassa, M. and Busalacchi, A.J. 2003. El Niño Tropical Pacific Ocean surface current and temperature evolution in 2002 and outlook for early 2003. *Geophys. Res. Lett., 30,* doi:10.1029/2003GL017096.

Large, W.B. 2006. Surface Fluxes for practitioners of Global Ocean Data Assimilation. *Ocean weather forecasting: An integrated view of oceanography.* E. P. Chassignet and J. Verron, Eds., 229–270.

Lee, S.K., Enfield, D.B. and Wang, C. 2005. Ocean general circulation model sensitivity experiments on the annual cycle of Western Hemisphere Warm Pool. *J. Geophys. Res., 110,* doi:10.1029/2004JC002640.

Levitus, S. 1982. *Climatological atlas of the world ocean.* U.S. Dept. of Commerce, National Oceanic and Atmospheric Administration, Rockville, 173 pp.

Liu, W.T. and Gautier, C. 1990. Thermal Forcing on the Tropical Pacific from Satellite Data. *J. Geophys. Res., 95,* 13209–13217.

Lorbacher, K., Dommenget, D., Niiler, P.P. and Kohl, A. 2006. Ocean mixed layer depth: A subsurface proxy of ocean-atmosphere variability. *J. Geophys. Res., 111,* doi:10.1029/2003JC002157.

Mackas, D.L., Strub, P.T., Thomas, A.C. and Montecino, V. 2006. Eastern Ocean Boundaries Pan-regional overview. *The sea, Vol. 14A, The Global Coastal Ocean*. A. R. Robinson and K. H. Brink, Eds., 21–59.

McClain, C.R., Feldman, G.C. and Hooker, S.B. 2004. An overview of the SeaWiFS project and strategies for producing a climate research quality global ocean bio-optical time series. *Deep-Sea Res. Part II, 51,* 5–42.

McClain, C.R., Christian, J.R., Signorini, S.R., Lewis, M.R., Asanuma, I., Turk, D. and Dupouy-Douchement, C. 2002. Satellite ocean-color observations of the tropical Pacific Ocean. *Deep-Sea Res. Part II, 49,* 2533–2560.

Mcphaden, M.J., Cronin, M.F. and Mcclurg, D.C. 2008. Meridional structure of the seasonally varying mixed layer temperature balance in the eastern tropical Pacific. *J. Clim., 21,* 3240–3260.

Montecino, V., Strub, P.T., Tarazona, J., Chavez, F.P., Thomas, A.C. and Baumgartner, T. 2006. Bio-physical interactions off western South America. *The sea, Vol. 14A, The Global Coastal Ocean*. A. R. Robinson and K. H. Brink, Eds., 329–390.

Muñoz, R.C. and Garreaud, R.D. 2005. Dynamics of the low-level jet off the west coast of subtropical South America. *Mon. Wea. Rev., 133,* 3661–3677.

Norris, J.R. 1998. Low cloud type over the ocean from surface observations. Part II: Geographical and seasonal variations. *J. Clim., 11,* 383–403.

Peixoto, J.P. and Oort, A.H. 1992. *Physics of climate*. American Institute of Physics, New York, 520 pp.

Pennington, J.T., Mahoney, K.L., Kuwahara, V.S., Kolber, D.D., Calienes, R. and Chavez, F.P. 2006. Primary production in the eastern tropical Pacific: A review. *Prog. Oceanogr, 69,* 285–317.

Reed, R.K. 1977. On estimating insolation over the ocean. *J. Phys. Oceanogr., 7,* 482–485.

Renault, L., Dewitte, B., Falvey, M., Garreaud, R., Echevin, V. and Bonjean, F. 2009. Impact of atmospheric coastal jet off central Chile on sea surface temperature from satellite observations (2000-2007). *J. Geophys. Res., 114,* doi:10.1029/2008JC005083.

Rodríguez-Rubio, E. and Stuardo, J. 2002. Variability of photosynthetic pigments in the Colombian Pacific Ocean and its relationship with the wind field using ADEOS-I data. *Proc. Indian Acad. Sci., 111,* 227–236.

Rodríguez-Rubio, E., Schneider, W. and Abarca del Río, R. 2003. On the seasonal circulation within the Panama Bight derived from satellite observations of wind, altimetry and sea surface temperature. *Geophys. Res. Lett., 30,* doi:10.1029/2002GL016794.

Rutllant, J. 2004. Aspectos de la circulación atmosférica de gran escala asociada al ciclo ENOS 1997-1999 y sus consecuencias en el régimen de precipitación en Chile central. *El Niño-La Niña 1997-2000: su efecto en Chile*. Avaria, S., Carrasco, J., Rutland, J. and Yañez, E. Eds., 61–76.

Smith, S.D. 1980. Wind stress and heat flux over ocean in gale force winds. *Journal Physical Oceanography, 10,* 709–726.

Smith, S.D. 1988. Coefficients for sea surface wind stress, heat flux, and wind profiles as a function of wind speed and temperature. *J. Geophys. Res., 93,* 15467–15472.

Sobarzo, M., Bravo, L., Donoso, D., Garcés-Vargas, J. and Schneider, W. 2007. Coastal upwelling and seasonal cycles that influence the water column over the continental shelf off central Chile. *Prog. Oceanogr., 75,* 363–382.

Soto-Mardones, L., Pares-Sierra, A. and Durazo, R. 2004. Ekman modulation of the sea-surface temperature on the Eastern South Pacific. *Deep-Sea Res. Part II, 51,* 551–561.

Takahashi, 2005. The Annual Cycle of Heat Content in the Peru Current Region. *J. Clim., 18,* 4937–4954.

Taylor, P.K. 2000. Intercomparison and validation of ocean-atmosphere energy flux fields. Joint WCRP/SCOR Working Group on Air Sea Fluxes. 305 pp.

Thiel, M. et al. 2007. The Humboldt Current System of northern and central Chile. *Oceanography and Marine Biology, 45,* 195–344.

Trenberth, K.E. 1997. The Definition of El Niño. Bull. Amer. Meteorol. Soc., 78, 2771–2777.

Trenberth, K.E. et al. 2007. Observations: Surface and Atmospheric Climate Change. *Climate change 2007: The Physical Science Basis. Contribution of Working Group I to the Fourth Assessment Report of the Intergovernmental Panel on Climate Change*. Solomon, S., Qin, D., Manning, M., Chen, Z., Marquis, M., Averyt, K.B., Tignor, M. and Miller, H.L. Eds., 235–336.

Vialard, J., Menkes, C., Boulanger, J.P., Delecluse, P., Guilyardi, E., McPhaden, M.J. and Madec, G. 2001. A model study of oceanic mechanisms affecting equatorial Pacific sea surface temperature during the 1997-98 El Niño. *J. Phys. Oceanogr., 31,* 1649–1675.

Waliser, D.E. and Gautier, C. 1993. A Satellite-Derived Climatology of the ITCZ. J. Clim., 6, 2162–2174.

Wallcraft, A.J., Kara, A.B., Hurlburt, H.E., Chassignet, E.P. and Halliwell, G.H. 2008. Value of bulk heat flux parameterizations for ocean SST prediction. *Journal of Marine Systems, 74,* 241–258.

Wang, C.Z. and Fiedler, P.C. 2006. ENSO variability and the eastern tropical Pacific: A review. *Prog. Oceanogr., 69,* 239–266.

Wang, W.M. and McPhaden, M.J. 1999. The surface-layer heat balance in the equatorial Pacific Ocean. Part I: Mean seasonal cycle. *J. Phys. Oceanogr., 29,* 1812–1831.

Wang, W.M. and McPhaden, M.J. 2000. The surface-layer heat balance in the equatorial Pacific Ocean. Part II: Interannual variability. *J. Phys. Oceanogr., 30,* 2989–3008.

Wang, W.M. and McPhaden, M.J. 2001a. What is the mean seasonal cycle of surface heat flux in the equatorial Pacific? *J. Geophys. Res., 106,* 837–857.

Wang, W.M. and McPhaden, M.J. 2001b. Surface Layer Temperature Balance in the Equatorial Pacific during the 1997-98 El Niño and 1998-99 La Niña. *J. Clim., 14,* 3393–3407.

Worley, S.J., Woodruff, S.D., Reynolds, R.W., Lubker, S.J. and Lott, N. 2005. ICOADS release 2.1 data and products. Int. J. Climatol., 25, 823–842.

Yu, L. and Weller, R. 2007. Objectively Analyzed Air–Sea Heat Fluxes for the Global Ice-Free Oceans (1981–2005). *Bull. Amer. Meteorol. Soc., 88,* 527–539.